Intensity of light field and electron concentration in the laser-induced plasma in a droplet of water aerosol exposed to a femtosecond laser pulse. Geometric optics analysis

V.P. Kandidov and V.O. Militsin

M.V. Lomonosov Moscow State University

Received October 2, 2003

The geometric optics approach is used to analyze propagation of a femtosecond laser pulse in a water microdroplet. The dynamics of spatial distribution of light intensity and electron concentration over the laser-induced plasma in a microdroplet exposed to a femtosecond laser pulse is investigated. The calculations have been carried out with the help of the ray-tracing technique. Shadow face reflection and ray interference that appear due to aberrated focusing are taken into account in the numerical simulation. The spatial distribution of light intensity obtained for droplets with the size larger than 20 μm is close to that calculated by the Lorenz–Mie theory. It is shown that at the pulse duration of 45 fs (a Ti:Sapphire laser) and the peak intensity of 10^{11} W/cm^2 an optical breakdown occurs in a water microdroplet of 30 μm in radius.

Introduction

The scope of a rapidly developing femtosecond nonlinear atmospheric optics involves a wide range of problems on the interaction of $20–100 \cdot 10^{-15}$ s-duration laser pulses having the peak power of $10^{10}–10^{12}$ W with atmospheric constituents.[1] Nonlinear optics of atmospheric aerosol occupies a significant place among these problems. The interaction of a high-power laser radiation with aerosol particles may considerably affect the phenomenon of laser pulse filamentation and generation of supercontinuum, which is now considered as a promising source for broadband sensing of the atmosphere.[2] Aerosol microparticles are not only an essential factor affecting propagation of laser pulses in atmospheric air, but also an independent object of study in atmospheric monitoring. Therefore, the interaction of high-power femtosecond laser pulses with aerosol particles is too a complicated problem, whose solution is now quite urgent.

Most papers concerning nonlinear optical interaction of laser radiation with an aerosol particle that were published in the 1980s–1990s considered pulses of micro- and nanosecond duration or the quasi-continuous emission mode.[3] In one of the first papers dealing with the femtosecond range of pulse duration, Zemlyanov and Geints[4] have calculated the process of establishing the whispering gallery modes of the light field in a spherical droplet. Boutou and Hill in a series of papers[5–7] have studied theoretically and experimentally the emission from multiphoton processes in an aerosol particle. Fluorescence was observed in ethanol and methanol droplets, and white-light emission was observed in water aerosol droplets at laser-induced breakdown inside a particle. The spatial distributions of the internal field intensity, electron concentration in laser-induced plasma, density of fluorescing sources, and the directional pattern of the emitted radiation have been calculated.

In theoretical investigations of the nonstationary internal field, various methods of solution of the Maxwell equation in a particle are used: finite difference method in the (3D+1) space, which is direct solution of the initial equations,[8] Fourier analysis method or, in other words, the Lorenz–Mie method, which considers a superposition of Mie solutions for all harmonics of the frequency spectrum of the laser pulse,[9] the method of resolution of the electromagnetic field of a spherical particle into eigenmodes, which is most efficient in the problems of nonlinear scattering by an aerosol particle.[4] These methods are computationally time consuming, and their application to the problems of nonlinear optics of atmospheric aerosol is not always justified.

In this paper, the geometric optics approximation is used for analysis of the internal field of a spherical particle exposed to a femtosecond laser pulse.

Geometric optics calculation of the field inside a particle

The geometric-optics approximation is applicable to calculation of the field inside a particle, if the radius of the first Fresnel zone determined near the shadow surface is much larger than the particle radius R. This condition leads to the inequality

$$R >> 2\lambda_0. \qquad (1)$$

In the case of a Ti:Sapphire laser ($\lambda_0 = 0.8$ μm) condition (1) is fulfilled for most of the atmospheric aerosol droplets. The paraxial estimation of the focusing properties of a spherical droplet gives that the focal length of its front illuminated surface is

$$F_1 = R\frac{n_{\text{drop}}}{(n_{\text{drop}} - 1)}. \qquad (2)$$

For water (refractive index $n_{\text{drop}} = 1.33$) $F_1 \approx 4R$, and the increase in the intensity due to focusing on

0235-6880/04/01 46-08 $02.00

the illuminated surface manifests itself partly inside the droplet. For the wave reflected from the shadow droplet surface, the focal length is

$$F_2 = R\frac{(2 - n_{\text{drop}})}{(3 - n_{\text{drop}})}. \quad (3)$$

The following inequality is true: $F_2 < 2R$, thus indicating a significant increase in the intensity of the internal field due to focusing of the radiation reflected from the shadow surface of the droplet.

The geometric optics analysis employs the ray tracing method, according to which a uniform grid is introduced near the illuminated droplet surface in the plane normal to the radiation propagation direction and the intensity distribution and the wave front of the incident beam are specified on it. A ray with the weight m proportional to the intensity of incident radiation is emitted from every point of the computational grid. The ray is directed normally to the wave front at this point. Then the spatial displacement and the phase change are considered for each ray individually with the following calculation of ray reflection or refraction at the interface between media.

In this paper, we study, in the scalar approximation, the incidence of a plane wave, which allows us to pass on to the axially symmetric consideration. In this case, a uniform (over the radius) distribution is specified for the rays with the specific weight m_p:

$$m_p = ph, \quad (4)$$

where h is the grid step; p is the distance to the axis (impact parameter). The set of rays with the close values of the impact parameter $[p; p + \mathrm{d}p]$ form a ray tube (Fig. 1). In the axially symmetric case, a ray beyond the droplet is a side surface of a cylinder with the radius p, while inside the droplet it is a side surface of a cone, whose radius $r(z, p)$ varies with the coordinate z and parametrically depends on p. Correspondingly, a ray tube beyond the droplet is a ring volume confined between two cylinders with the radii differing by $\mathrm{d}p$, while inside the droplet it is a volume between two cones with the radii r and $r + \mathrm{d}r$.

The incidence angle of the ray θ is connected with the impact parameter by a simple relationship

$$p = R\sin\theta. \quad (5)$$

At refraction or a reflection from the air/water interface, the ray weight m_p changes according to the Fresnel formulas.

The parts of the ray trajectory inside the droplet are calculated analytically. Thus, for the part from the entrance into the droplet to the first reflection the radial r and the longitudinal z ray coordinates and the impact parameter p are related as

$$r(z,p) = p - [p\cot\theta + z]\tan(\theta - \psi), \quad (6)$$

where the refraction ψ and incidence θ angles can be uniquely expressed through the parameter p.

In the process of propagation inside the droplet, the area of the cross section of the ray tube changes. Since there is no energy exchange between tubes, the intensity $I_{\text{int}}(z, p)$ in the pth tube can be found from the relationship

$$I_{\text{int}}(z,p)\, r(z,p)\, \mathrm{d}r = I_{\text{ext}} \sum_{j=J_p}^{J_p+N_p} m_j, \quad (7)$$

where I_{ext} is the intensity of the incident wave; $J_p = [p/h]$ is the number of the ray corresponding to the impact parameter p; $N_p = [\mathrm{d}p/h]$ is the number of rays in the pth tube and $\mathrm{d}r$ is the width of the ray tube inside the droplet (see Fig. 1). As z increases, the area of the cross section of the ray tube decreases and the intensity $I_{\text{int}}(z, p)$ in it increases.

In analyzing the intensity distribution inside the droplet, it is convenient to introduce a radius-uniform grid with the step g in the cross sections for ray tubes. In this case, for any coordinate z the thickness of the ray tube inside the droplet is assumed fixed and equal to the grid step $\mathrm{d}r = g$, where $\mathrm{d}r \gg h$. Then for calculation of the intensity $I_{\text{int}}(z, p)$, the rays, whose radial coordinate falls within the range $[r; r + g]$, are summed up. This algorithm in accordance with Eq. (7) can be interpreted as a fit of the incident ray tube with such an impact parameter $[p(r, z); p(r, z) + \mathrm{d}p(r, z)]$ that it falls within the grid cell $[r; r + g]$ at the distance z chosen.

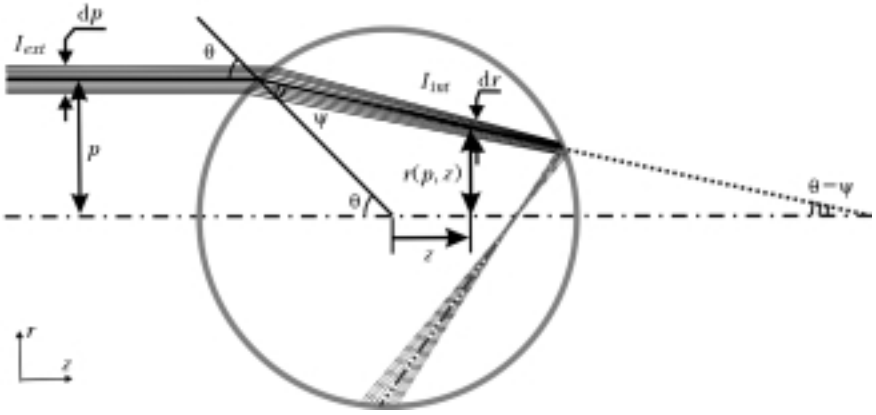

Fig. 1. Ray propagation inside a water droplet. The radiation is incident from left to right.

In this paper, we use the ray grid with the step $h = 10^{-5}R$ and the ray tube grid with the step $dr = 10^{-2}R$, which allowed us to sufficiently accurate calculate the intensity distribution over the cross sections with the spatial resolution of $10^{-2}R$. Thus, for the droplet of $R = 30$ μm in radius, the error in the intensity in the cross section $z = 0$ does not exceed 1%.

The intensity distribution due to contraction of ray tubes, that is, focusing by the illuminated droplet surface is depicted in Fig. 2*a* for the central $z = 0$ cross section. The peak intensity due to focusing in this cross section $I_{\text{int}}(z = 0,\ r = 0)$ is 1.6 times higher than that of the incident radiation I_{ext}.

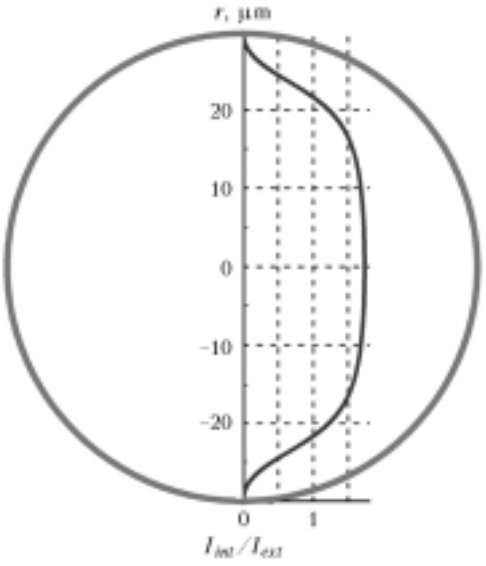

a

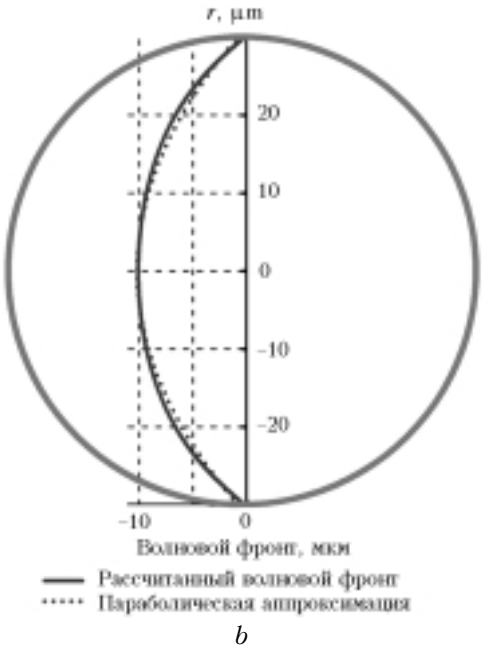

b

Fig. 2. Intensity distribution (*a*) and wave front (*b*) due to focusing at the illuminated surface in the central, $z = 0$, cross section of the droplet: calculated wave front (—) and parabolic approximation (⋆⋆⋆⋆).

To determine the phase change in the ray tubes, the optical path $l_p(z)$ is calculated. The phase change in the pth ray tube $\varphi(z, p)$ is determined from the mean optical path of the component rays taken with the corresponding weights:

$$\varphi(z,p) = \frac{2\pi}{\lambda_0} \sum_{j=J_p}^{J_p+N_p} m_j l_j(z) \Bigg/ \sum_{j=J_p}^{J_p+N_p} m_j. \qquad (8)$$

Figure 2*b* depicts the calculated profile of the wave front in the droplet of radius $R = 30$ μm for the central droplet cross section $z = 0$ along with its approximation by the parabolic wave front obtained by the least squares method (dashed curve). The radius of curvature of the parabolic wave front is ~ 77 μm, while that estimated by Eq. (2) is ~ 90 μm. The difference in the radii of curvature and the deviation of the real phase profile from the parabolic one are consequences of aberrations at focusing by a spherical surface. As a cross section located farther in the shaded part of the sphere is considered, the aberration effects become more pronounced.

The dependence of the radial ray coordinate r on the impact parameter p in the plane at the distance $z = 0.9R$ from the central cross section is shown in Fig. 3. It can be seen that at $p \geq 0.85$ there is an area, where one value of the coordinate r corresponds to two values of the impact parameter p and, correspondingly, to two ray tubes.

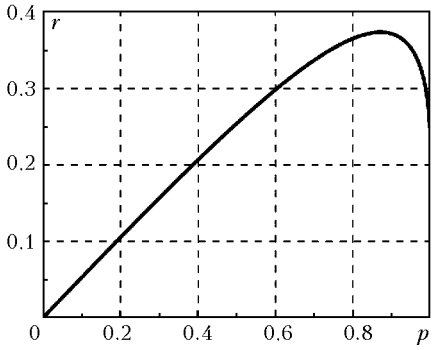

Fig. 3.

In this area, the intensity redistribution is formed due to interference of rays after refraction on the illuminated droplet surface. The area of the interference of the ray tubes at their intersection is shown in Fig. 4*a*. The longitudinal dimension of this area in the droplet with the radius of 30 μm is about 10 μm, while the lateral dimension is 4 μm.

At the point of intersection of K ray tubes with the impact parameters p_k, the intensity is

$$I_{\text{int}}(z,r) = \left[\sum_{k=1}^{K} \sqrt{I_{\text{int}}(z,p_k)}\, \exp[i\varphi(z,p_k)]\right]^2. \qquad (9)$$

The number of the intersecting ray tubes K depends on the coordinate of the point inside the droplet (z, r). The impact parameter p_{kr}, at which the

derivative $dp/dr = 0$, corresponds to the caustic, and the geometric optics approximation in this area is inapplicable to calculation of the intensity. This value of p_{kr} corresponds to a wide-aperture angle at "rainbow" formation.

Near the droplet axis, the intensity of the internal field I_{int} achieves the values about $4I_{ext}$ due to focusing by the illuminated surface. In Fig. 4*b* one can clearly see the zone of the enhanced intensity forming a ring near the external droplet boundary with the structure characteristic of an interference pattern. The external droplet boundary in the analyzed surface is shown by a dashed line in Fig. 4*b*. In this area the intensity at the interference peak increases by ~20 times as compared with the incident wave, and the growth of the field at the caustic boundary can be estimated by averaging over the area with the characteristic size about the wavelength λ_0.

In analysis of femtosecond pulse propagation in a microdroplet, we restrict our consideration to single reflection from the shadow surface. This approximation is valid, if the pulse duration τ_p is shorter than the time τ_g needed to the light wave to cross the spherical droplet:

$$\tau_g \le \frac{2R}{c_0 n_{drop}}, \qquad (10)$$

where c_0 is the speed of light.

At the pulse duration $\tau_p \sim \tau_g$, its leading edge after reflection from the shadow surface is focused inside the droplet volume and interferes with the trailing edge. For the droplet of 30 μm in radius, the characteristic time is $\tau_g \approx 150$ fs. Figure 5 shows, as an illustration, continuous-tone pattern of the field intensity inside a droplet with regard for single reflection from the shadow surface for a square-shaped pulse. Dark parts correspond to higher intensity. The maximum increase in the intensity is achieved at the droplet axis in a cylindrical area about 10 μm long with the cross section of 3 μm. This area is located about 7 μm far from the shadow surface, which agrees with the focal length $F_2 \approx 12$ μm estimated by Eq. (3). The maximum increase in the intensity is about 200 times as compared to that of the incident wave. This result suggests that at propagation of a high-power femtosecond laser pulse in this area we should expect an essential manifestation of the nonlinear optical effects and pulse self-action.

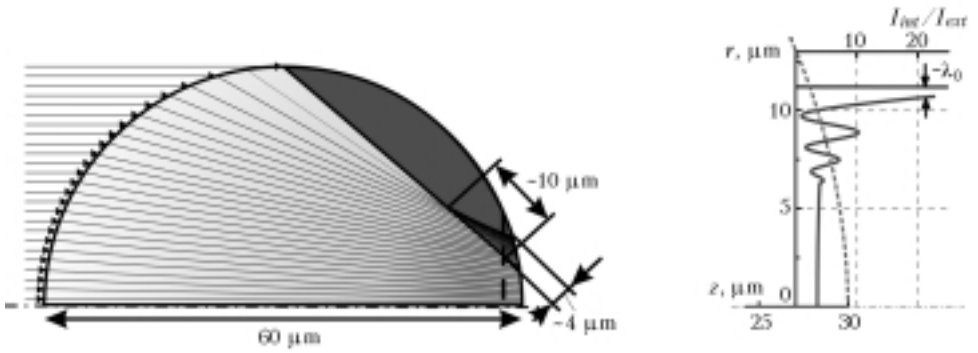

a *b*

Fig. 4. Interference area inside the droplet: ray paths inside the droplet that determine the intensity redistribution (*a*); intensity distribution at the distance $z = 0.9R$ from the droplet center (*b*).

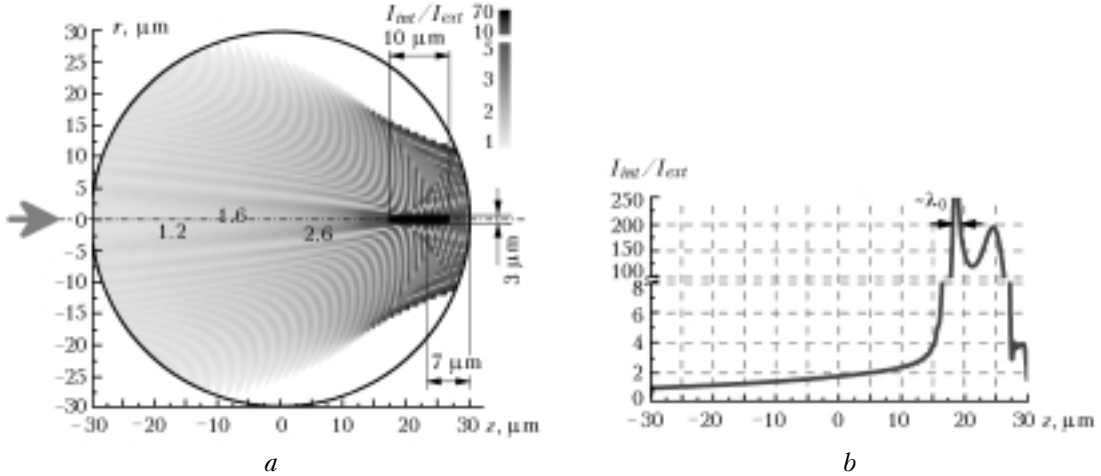

a *b*

Fig. 5. Intensity distribution inside the droplet with regard for single reflection from the shadow surface: in the volume (*a*), on the axis ($r = 0$) (*b*).

Dynamics of the field inside a particle

To consider the dynamics of the intensity at propagation of a femtosecond laser pulse inside a droplet, we used the values of the phase change $\varphi(z, p)$ pre-calculated for every ray tube. Thus, for a Gaussian pulse with the input envelope

$$I_{\text{ext}}(t) = I_0 \exp\left[-4\ln 2\left(\frac{t}{\tau_{\text{L}}}\right)^2\right], \qquad (11)$$

where τ_{L} is the full duration at half maximum, the time dependence of the intensity in the pth ray tube is determined by the following expression:

$$I_{\text{int}}(z,p,t) = I_{\text{int}}(z,p)\exp\left[-4\ln 2\left(\frac{t-\varphi(z,p)/\omega}{\tau_{\text{L}}}\right)^2\right]. \qquad (12)$$

Here ω is the carrier circular frequency; the intensity $I_{\text{int}}(z, p)$ is given by Eq. (7). Thus, as the longitudinal coordinate z varies in the pth ray tube, the pulse is delayed by the radiation propagation time $\varphi(z, p)/\omega$.

Figure 6 depicts the radiation intensity distributions of a Gaussian pulse $\tau_{\text{L}} = 45$ fs-long for some characteristic moments in time. The zero time $t = 0$ is the time, when the peak of the pulse at the droplet axis passes through the illuminated surface ($z = -R$).

At the time $t = 130$ fs, when the pulse peak is roughly at the droplet center $z = 0$, the intensity increases due to radiation focusing at the droplet axis (Fig. 6*a*). During the further propagation, a ring interference area is formed, and the increase of the intensity at the peaks of the interference pattern achieves ~ 20 times (Fig. 6*b*). At the time $t = 270$ fs the pulse peak reaches the shadow surface at the droplet axis (Fig. 6*c*). As this occurs, the pulse trailing edge continues to form the ring interference area, and the reflected part of the leading edge is focused at the axis 6 μm far from the shadow surface. The interference pattern also is formed in the region of overlap of the leading and trailing pulse edges. For a Gaussian pulse the intensity increase in it is much less than that in the focusing area.

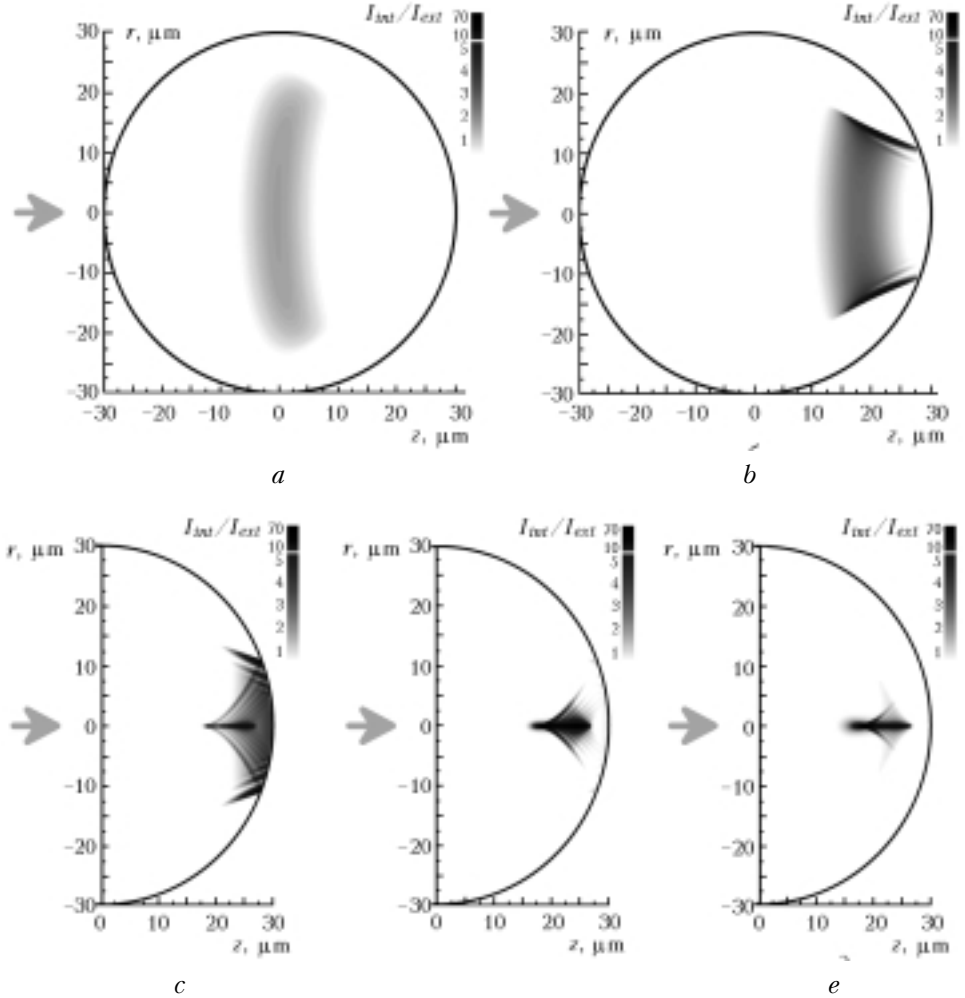

Fig. 6. Intensity distribution of the pulse of $\tau_{\text{L}} = 45$ fs-duration inside a water droplet at different time t, in fs: 130 (*a*), 210 (*b*), 270 (*c*), 300 (*d*), and 330 (*e*). The pulse is incident from left to right along the arrow. The time is measured from the instant when the peak of the pulse at the droplet axis ($r = 0$) crosses the illuminated surface ($z = -R$).

At the further propagation of the reflected pulse, its central, in time, layers reach the area of sharpest focusing, and the maximum intensity in this area is roughly 100 times as high as the intensity of the incident radiation I_0 (Fig. 6*d*). Then (t = 330 fs) pulse blooming begins, and the intensity decreases (Fig. 6*e*). The area, where the intensity exceeds that of the incident radiation, contracts considerably as compared to earlier instants. The intensity in the zone of maximum focusing also decreases and roughly 40 times exceeds that of the incident radiation at t = 330 fs. The spatial blooming of the pulse continues, and at t = 360 fs the intensity in the volume droplet does not exceed the intensity of the incident radiation I_0.

The results presented suggest that for the pulses no longer in space than the droplet diameter there are two zones of a considerable increase in the intensity. Manifestation of the nonlinear optical effects and formation of the laser-induced plasma are most probable in these zones. One zone is the ring interference area near the shadow surface of the droplet, where the intensity is as high as $20\,I_0$, and the other one is the zone of focusing of radiation reflected from the shadow surface, where the intensity is roughly as high as $100\,I_0$. The time dependence of the intensity in these zones is almost identical to the time profile of the incident pulse. The second zone is formed with some lag determined by the time of propagation of the reflected pulse. For the considered pulse of τ_L = 45 fs-duration and a droplet with the radius of R = 30 μm this lag is about 90 fs.

Formation of plasma

Laser-induced electron plasma is generated during pulse propagation inside the water droplet. In the zones of maximum increase in the intensity, we should expect the highest electron concentration. To describe formation of the electron plasma, we used a model accounting for multiphoton and cascade ionization and recombination of plasma.[10] The rate equation describing the dynamics of the electron density $\rho(r, z, t)$ has the following form:

$$\frac{d\rho}{dt} = \left(\frac{d\rho}{dt}\right)_{mp} + \eta_{casc}\rho - \eta_{rec}\rho^2, \qquad (13)$$

where the first term in the right-hand side of the equation describes the multiphoton ionization, while the second is for the cascade ionization, and the third one describes recombination.

To take into account multiphoton ionization under the exposure to a laser field in water, we use Keldysh approximation. For ionization of a molecule with the ionization energy ΔE, the needed number of photons can be estimated as $k = \langle \Delta E/(\hbar\omega) + 1 \rangle$. For a pulse from a Ti:Sapphire laser ($\lambda_0 = 0.8$ μm) and the water molecule with ΔE = 6.5 eV, k = 5. According to this approximation, the rate of multiphoton ionization is

$$\left(\frac{d\rho}{dt}\right)_{mp} \approx \frac{\omega}{9\sqrt{\pi}}\left(\frac{m'\omega}{\hbar}\right)^{3/2}\left[\frac{e^2}{16m'\Delta E\omega^2 c_0\varepsilon_0 n_{drop}}I\right]^k \times$$

$$\times \exp\left(\frac{2\Delta E}{\hbar\omega}\right)\mathrm{erf}\left(\sqrt{2k - \frac{2\Delta E}{\hbar\omega}}\right), \qquad (14)$$

where m' is assumed equal to the electron half-mass, $m' = m_e/2$; I is the radiation intensity. The rate of cascade ionization is determined as

$$\eta_{casc} = \frac{1}{\omega^2\tau_{col}^2 + 1}\left[\frac{e^2\tau_{col}}{c_0 n_{drop}\varepsilon_0 m_e \Delta E}I - \frac{m_e\omega^2\tau_{col}}{M}\right], \qquad (15)$$

where τ_{col} = 1 fs is the time of electron–molecule collisions; $M = 3\cdot10^{-26}$ kg is the mass of a water molecule. The coefficient at the term describing recombination was assumed constant and equal to $\eta_{rec} = 2\cdot10^{-9}$ cm^3/s. The following calculation shows that at the time of femtosecond pulse propagation in a water microdroplet the effect of recombination on the formation of plasma is insignificant.

The electron density $\rho(z, r, t)$ at a given droplet point (z, r) was calculated through solution of Eq. (13) by the Runge–Kutta method using numerically obtained time dependence of the intensity $I_{int}(z, r, t)$.

Figure 7 shows the continuous-tone patterns of the electron concentration in the central longitudinal cross section for a water microdroplet of the radius R = 30 μm and the input pulse (11) with the duration τ_L = 45 fs and peak intensity $I_0 = 3\cdot10^{11}$ W/cm^2 for some characteristic instants. The calculation was carried out with the time step Δt = 1 fs and the spatial resolution $g = 0.01R$.

As the pulse penetrates the droplet, the probability of ionization is low, and the plasma with the concentration no higher than $10^{-14}\rho_0$, where $\rho_0 = 3.34\cdot10^{22}$ cm^{-3} is the equilibrium concentration of water molecules, is formed only in the front part of the droplet. Then the ionization zone extends, and by the time t = 130 fs the electron concentration at the droplet center increases up to $10^{-11}\rho_0$ under the effect of the growing field (Fig. 7*a*). The electron concentration is accumulated with time and in any part of the droplet the peak of the electron density is delayed from the peak of the internal field. When the interference increase of the intensity near the rear wall of the microdroplet starts (t = 210 fs), ionization occurs almost in the entire droplet (Fig. 7*b*). The electron concentration in the ring area, where the intensity is maximum, is $\rho_{max} = 3\cdot10^{19}$ cm^{-3}.

After reflection from the shadow surface, the pulse propagates backwards, thus causing the further increase of the electron density in the axial zone (t = 270 fs, Fig. 7*c*). The highest electron density is achieved in the zone of maximum focusing of the reflected radiation at t = 330 fs (Fig. 7*d*), and for the chosen droplet and pulse parameters it is $\rho_{max} = 3\cdot10^{22}$ cm^{-3}, that is, about 1% of the equilibrium concentration of water molecules $\rho_{max} \approx 10^{-2}\rho_0$. Thus, at the peak intensity of the input pulse higher than $I_0 = 3\cdot10^{11}$ W/cm^2, the optical breakdown occurs in the droplet.[11]

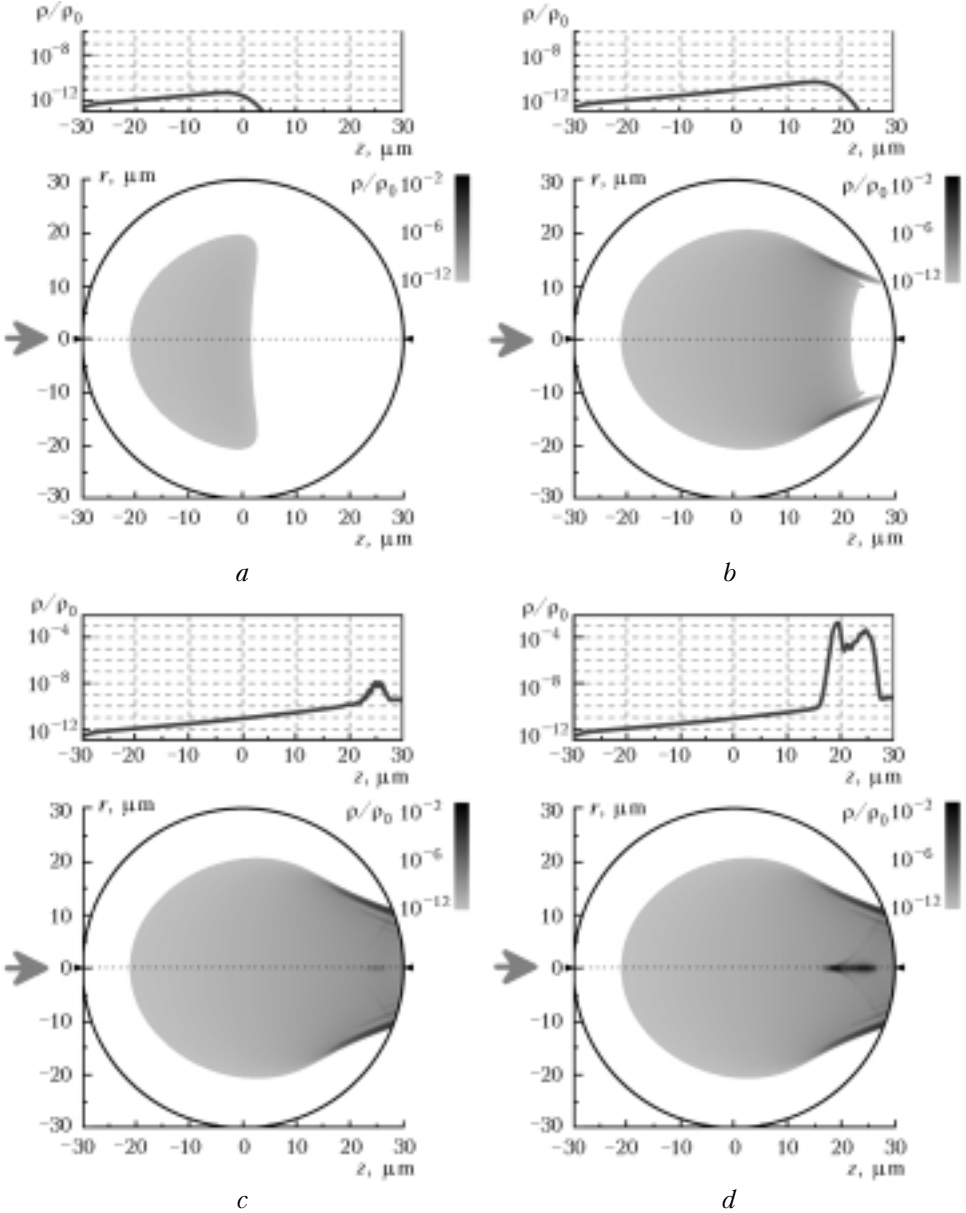

Fig. 7. Electron plasma density inside a water droplet at propagation of a pulse of $\tau_L = 45$ fs duration and peak intensity $I_0 = 3 \cdot 10^{11}$ W/cm^2 at different time t, in fs: 130 (*a*), 210 (*b*), 270 (*c*), and 330 (*d*). Time is measured from the instant, when the pulse peak at the droplet axis ($r = 0$) penetrates the illuminated surface ($z = -R$).

Figure 8 depicts the time dependence of the electron concentration in the laser-induced plasma at the axis in the zone of maximum focusing of the reflected radiation at the distance $\Delta z = 11$ μm from the shadow surface. The nonuniform increase of the plasma concentration is explained by the fact that strong ionization first occurs at the forward propagation of the pulse, and its following drastic increase is caused by the backward propagation of the central, in time, layers of the pulse after reflection from the shadow surface.

Once the pulse has been terminated, the electron concentration decreases tenfold for the time of about 10 ps. Thus, recombination of the plasma for the time of propagation of a femtosecond laser pulse inside the microdroplet is insignificant.

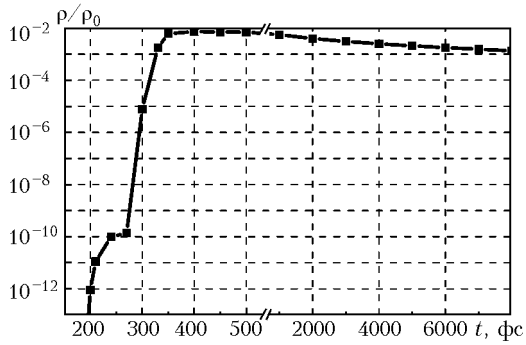

Fig. 8. Electron plasma density at the droplet axis ($r = 0$) at the distance $z = 18$ μm as a function of time in the case of propagation of a pulse with the duration $\tau_L = 45$ fs and peak intensity $I_0 = 3 \cdot 10^{11}$ W/cm^2.

Conclusions

1) Based on the ray tracing method, the approach has been developed to numerical investigation of the light field distribution inside an aerosol droplet exposed to a femtosecond laser pulse. The method is applicable to droplets, whose radii meet the condition $R \gg 2\lambda_0$. The pulse duration τ_p in this case is bounded above by the inequality

$$\tau_p < \frac{2R}{c_0 n_{drop}}.$$

The method accounts for the effect of radiation focusing by the illuminated droplet surface, field interference during the forward propagation of the pulse through the droplet and at reflection from the shadow surface.

2) Using a droplet of 30 μm in radius as an example, we have shown that for radiation with the wavelength of 0.8 μm and pulse duration of 45 fs, the field intensity inside the droplet increases roughly fourfold due to focusing by the illuminated surface, 20-fold at the interference maxima in the ring zone near the shadow surface, and 100-fold at focusing after reflection from the shadow surface. The estimates of the maximum increase in the intensity obtained for water droplets with the diameter larger than 20 μm agree with the results calculated by the Lorenz–Mie theory.

3) It has been established that at the peak intensity of the incident pulse of a Ti:Sapphire laser $I_0 = 3 \cdot 10^{11}$ W/cm^2, a zone of optical breakdown arises in an aerosol droplet due to multiphoton and cascade ionization. The maximum electron concentration in this zone achieves $\rho_{max} = 3 \cdot 10^{22}$ cm^{-3}, which is in a good agreement with the experimental data.[11]

The results obtained from analysis of the space-time distribution of the light filed intensity and the electron concentration in a water droplet can be used to study nonlinear optical processes of interaction of a femtosecond laser pulse with water-droplet aerosol.

Acknowledgments

This work was supported, in part, by the Russian Foundation for Basic Research (Grant No. 03–02–16939), ARL-ERO (Contract No. 62558–03–M–0029), and CRDF GAP (Grant No. RPO–1390–TO–03).

References

1. V.P. Kandidov, O.G. Kosareva, E.I. Mozhaev, and M.P. Tamarov, Atmos. Oceanic Opt. **13**, No. 5, 394–401 (2000).
2. J. Kasparian, M. Rodriguez, G. Méjean, J. Yu, E. Salmon, H. Wille, R. Bourayou, S. Frey, Y.-B. André, A. Mysyrowicz, R. Sauerbrey, J.-P. Wolf, and L. Wöste, Science **301**, No. 5629, 61–64 (2003).
3. V.V. Zuev, A.A. Zemlyanov, and Yu.D. Kopytin, *Nonlinear Atmospheric Optics* (Gidrometeoizdat, Leningrad, 1989), 256 pp.
4. A.A. Zemlyanov and Yu.E. Geints, Atmos. Oceanic Opt. **14**, No. 5, 316–325 (2001).
5. S.C. Hill, V. Boutou, J. Yu, S. Ramstein, J.-P. Wolf, Y. Pan, S. Holler, and R.K. Chang, Phys. Rev. Lett. **85**, No. 1, 54–57 (2000).
6. V. Boutou, C. Favre, S.C. Hill, W. Zimmer, M. Krenz, H. Lambrecht, J. Yu, R.K. Chang, L. Woeste, and J.-P. Wolf, Phys. Rev. Lett. **89**, No. 3, 035002-1 (2002).
7. V. Boutou, C. Favre, S.C. Hill, Y.L. Pan, R.K. Chang, and J.P. Wolf, Appl. Phys. B **75**, Nos. 2–3, 145–152 (2002).
8. P. Yang, K.N. Liou, M.I. Mishchenko, and B.-C. Gao, Appl. Opt. **39**, Issue 21, 3727–3737 (2000).
9. P.W. Barber and S.C. Hill, in: *Light Scattering by Particles: Computational Methods* (World Scientific, Singapore, 1990), pp. 140–233.
10. J. Noak and A. Vogel, IEEE J. Quantum Electron. **35**, No. 8, 1156–1167 (1999).
11. P.K. Kennedy, S.A. Boppart, D.X. Hammer, B.A. Rockwell, G.D. Noojin, and W.P. Roach, IEEE J. Quantum Electron. **31**, No. 12, 2250–2256 (1995).